

pubs.acs.org/JACS Article

# Stabilization of NbTe<sub>3</sub>, VTe<sub>3</sub>, and TiTe<sub>3</sub> via Nanotube Encapsulation

Scott Stonemeyer, Jeffrey D. Cain, Sehoon Oh, Amin Azizi, Malik Elasha, Markus Thiel, Chengyu Song, Peter Ercius, Marvin L. Cohen, and Alex Zettl



Cite This: J. Am. Chem. Soc. 2021, 143, 4563-4568



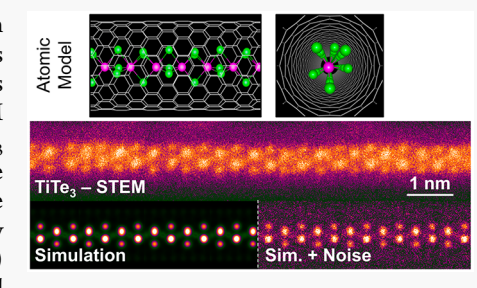
**ACCESS** 

Metrics & More



Supporting Information

ABSTRACT: The structure of MX<sub>3</sub> transition metal trichalcogenides (TMTs, with M a transition metal and X a chalcogen) is typified by one-dimensional (1D) chains weakly bound together via van der Waals interactions. This structural motif is common across a range of M and X atoms (e.g., NbSe<sub>3</sub>, HfTe<sub>3</sub>,TaS<sub>3</sub>), but not all M and X combinations are stable. We report here that three new members of the MX<sub>3</sub> family which are not stable in bulk, specifically NbTe<sub>3</sub>, VTe<sub>3</sub>, and TiTe<sub>3</sub>, can be synthesized in the few- (2–4) to single-chain limit via nanoconfined growth within the stabilizing cavity of multiwalled carbon nanotubes. Transmission electron microscopy (TEM) and atomic-resolution scanning transmission electron microscopy (STEM) reveal the chain-like nature and the detailed atomic structure. The synthesized



materials exhibit behavior unique to few-chain quasi-1D structures, such as few-chain spiraling and a trigonal antiprismatic rocking distortion in the single-chain limit. Density functional theory (DFT) calculations provide insight into the crystal structure and stability of the materials, as well as their electronic structure.

## **■ INTRODUCTION**

One of the primary objectives of nanoscience is the precise control over the processing–structure–property relationship intrinsic to traditional materials science. Recently, the concept of dimensionality and the engineering of materials' structure and properties via changes in dimensionality has emerged as an additional degree of freedom within this paradigm. To this end, isolation of single atomic planes (e.g., graphene<sup>1</sup> and the transition metal dichalcogenides<sup>2</sup>) and chains (e.g., transition metal trichalcogenides,<sup>3</sup> TMTs) from quasi-low-dimensional materials has been extremely fruitful. There is an ever-growing list of materials being isolated down to their fundamental van der Waals (vdW) building blocks, and existing low-dimensional materials (e.g., nanotubes, graphene) have been excellent templates for the synthesis and stabilization of new low-dimensional materials and structures.<sup>4-6</sup>

Carbon nanotubes (CNTs) and boron nitride nanotubes (BNNTs) have been used as nanoreaction vessels for the synthesis of a variety of materials, including elemental metals, halides, s, and chalcogenides. The CNT sheath enables the study of 1D nanostructures that are not air stable by protecting them from oxidation. In some cases, the nanoconfined growth can induce formation of crystal structures and morphologies unrealized in bulk counterparts, such as 1D HgTe, s, lelices in 1D cobalt iodide, and twisting in single-chain monochalcogenides. Encapsulation of materials inside small-diameter nanotubes has become a unique route toward new quasi-1D nanostructures.

The archetypal quasi-1D materials family is the TMTs, commonly referred to as MX<sub>3</sub> compounds, with M being a transition metal and X a chalcogen. Typically, for these

materials, 1D MX<sub>3</sub> chains are weakly coupled by interchain vdW interactions to form coherent, but highly anisotropic, three-dimensional crystals. The bulk synthesis and properties of the TMTs have been well explored, and they are canonical examples of superconductors and charge density wave materials. Recently, TMTs have also been isolated in the few- and single-chain limit, where they exhibit unique spiral chain structures and torsional instabilities induced by the added dimensional constraint. On the basis of chemical trends, one might expect the quasi-1D crystal structure seen in the TMTs to be present in all MX<sub>3</sub> compounds with M = Ti, Zr, Hf, Nb, or Ta and X = S, Se, or Te. While this holds true for many of the possible combinations (e.g., NbSe<sub>3</sub>, TaS<sub>3</sub>, HfTe<sub>3</sub>), specimens of many telluride-based TMTs have not been previously synthesized and are likely not stable in bulk. 17

Here, we demonstrate the successful synthesis of three previously unreported MX<sub>3</sub> TMT compounds: NbTe<sub>3</sub>, VTe<sub>3</sub>, and TiTe<sub>3</sub>. This is accomplished through nanoconfined growth within the cavity of multiwalled carbon nanotubes (MWCNTs). Depending upon the inner diameter of the encapsulating MWCNTs, specimens ranging from many chains, to few chains (2–4), and even single chain, can be isolated and studied. The MWCNT sheath stabilizes the chainlike morphology, enabling synthesis and characterization

Received: September 23, 2020 Published: December 1, 2020





with transmission electron microscopy (TEM) and aberration-corrected scanning transmission electron microscopy (STEM). It is found that few-chain specimens of the new TMTs can exhibit a coordinated interchain spiraling, while the single-chain limit exhibits a trigonal antiprismatic (TAP) rocking, behaviors seen previously in the few-chain limit of NbSe $_3$  and HfTe $_3$ . First-principles calculations give insight into the integral role that the encapsulating CNT plays in stabilization and provide information regarding the electronic structure of the new materials.

# ■ RESULTS AND DISCUSSION

The stabilized chains of NbTe<sub>3</sub>, VTe<sub>3</sub>, and TiTe<sub>3</sub> are synthesized within CNTs using a procedure similar to that outlined previously for NbSe<sub>3</sub> and HfTe<sub>3</sub>. Stoichiometric quantities of powdered transition metal and Te shot ( $\sim$ 450 mg total) together with 1–2 mg of end-opened MWCNTs (CheapTubes, 90% SW-DW CNTs) and  $\sim$ 5 mg/cm<sup>3</sup> (ampule volume) of I<sub>2</sub> are sealed under vacuum in a quartz ampule, heated in a uniform temperature furnace at 520–625 °C for several days, and then cooled to room temperature over 3–7 days.

Figure 1 shows high-resolution TEM images of representative samples from all three stabilized species encapsulated within MWCNTs in which their 1D, chain-like nature is evident. In Figure 1a,  $\sim$ 14 TiTe $_3$  chains are encapsulated within a 3.47 nm wide (inner diameter) MWCNT (number of enclosed chains estimated based on the carbon nanotube

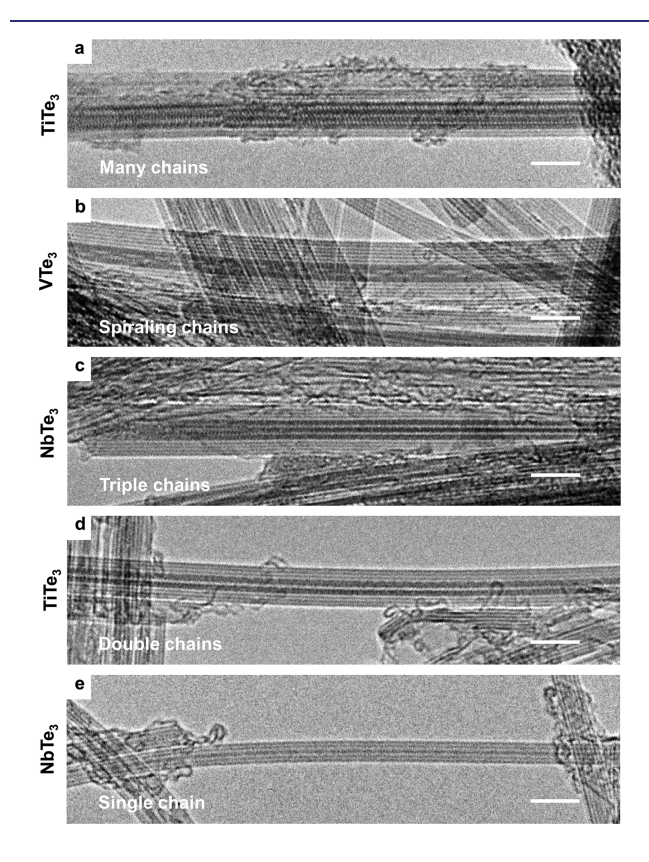


**Figure 1.** Representative samples of the many- to single-chain limit of  $TiTe_3$ ,  $VTe_3$ , and  $NbTe_3$ . Transmission electron microscopy images of (a) many chains of  $TiTe_3$ , (b) triple spiraling chains of  $VTe_3$ , (c) triple chains of  $NbTe_3$ , (d) double chains of  $TiTe_3$ , and (e) the single-chain limit of  $NbTe_3$ . All images are underfocused where atoms appear dark. Scale bars measure 5 nm.

diameter and a close-packing configuration of the chains). Figure 1b exhibits triple-spiraling chains of VTe<sub>3</sub> within a 2.46 nm MWCNT, while Figure 1c shows straight triple chains of NbTe<sub>3</sub> within a 2.57 nm wide MWCNT. Figure 1d shows a double-chain example of TiTe<sub>3</sub> within a 2.04 nm MWCNT, and Figure 1e highlights the single-chain limit of NbTe<sub>3</sub> encapsulated within a 0.99 nm wide MWCNT. These results demonstrate that a confined growth environment allows for the stabilization and characterization of many-, few-, and single-chain limits of NbTe<sub>3</sub>, VTe<sub>3</sub>, and TiTe<sub>3</sub>.

As seen in the TEM images in Figure 1, NbTe<sub>3</sub>, VTe<sub>3</sub>, and TiTe<sub>3</sub> adopt very similar behaviors when encapsulated, reminiscent of behaviors reported previously for NbSe3 and HfTe<sub>3</sub>. Spiraling in the triple-chain limit is evident as shown in Figures 1b and S1. Chemical analyses of the new materials by means of energy-dispersive X-ray spectroscopy (EDS) are shown in Figure 2. Figure 2a, 2b, and 2c shows annular darkfield scanning transmission electron microscope (ADF-STEM) images of few-chain specimen of NbTe<sub>3</sub>, VTe<sub>3</sub>, and TiTe<sub>3</sub>, respectively, as well as corresponding EDS line scans. EDS mapping is used to distribute the dose, and the maps are summed vertically to increase the signal-to-noise. The EDS line scans in Figure 2 a, 2b, and 2c confirm the distribution of the transition metal, Nb, V, or Ti respectively, and Te atoms across the few-chain crystal within the carbon nanotube. The EDS spectra collected from individual few-chain NbTe3, VTe3, and TiTe<sub>3</sub> are presented in Figure S2. The spectra clearly show peaks of Nb and Te for NbTe<sub>3</sub>, V and Te for VTe<sub>3</sub>, and Ti and Te for TiTe<sub>3</sub>.

The new TMT compositions are stable down to the singlechain limit. We examine the single-chain structure of these previously unreported chemistries using atomic-resolution annular dark field (ADF-) STEM imaging and STEM image simulation, as highlighted in Figure 3. The STEM simulations, with parameters matching those of the experimental imaging, are generated from the structures obtained by DFT calculations, as discussed in later sections. The left-hand section of the simulation shows the raw multislice output, and the right-hand section of the simulation incorporates noise from Poisson counting statistics according to the experimental electron beam dose. 18 The structure and contrast of atomic species observed in the simulations match the experimental images for each of the single TMT chains and highlight the ability of the ADF-STEM to distinguish the different atomic species in the single chains. In Figure 3a-c, single chains of NbTe<sub>3</sub>, VTe<sub>3</sub>, and TiTe<sub>3</sub> are seen encapsulated within a 1.11, 1.02, and 1.05 nm wide double-wall CNT, respectively. Figure 3d shows an atomic model of the single-chain TMT encapsulation process in a single-walled CNT, where the CNT clearly visible in the model may not be readily visible in the STEM images because of the contrast difference of the carbon atoms. The most striking aspect of all three compounds' structures in Figure 3a, 3b, and 3c is what appears to be the intrachain rocking of the Te ligands along the chain axis. Such a rocking was previously suggested by theory for few- and single-chain HfTe3 but not resolved experimentally due to the spatial resolution necessary to observe such a small structural variation. 16 The enhanced experimental resolution in the present study allows for direct confirmation of such a rocking distortion for NbTe<sub>3</sub>, VTe<sub>3</sub>, and TiTe<sub>3</sub>.

The intrachain rocking of the Te ligands distorts the trigonal prismatic (TP) chains into a trigonal antiprismatic (TAP) chain structure. This is relatively unsurprising for the single

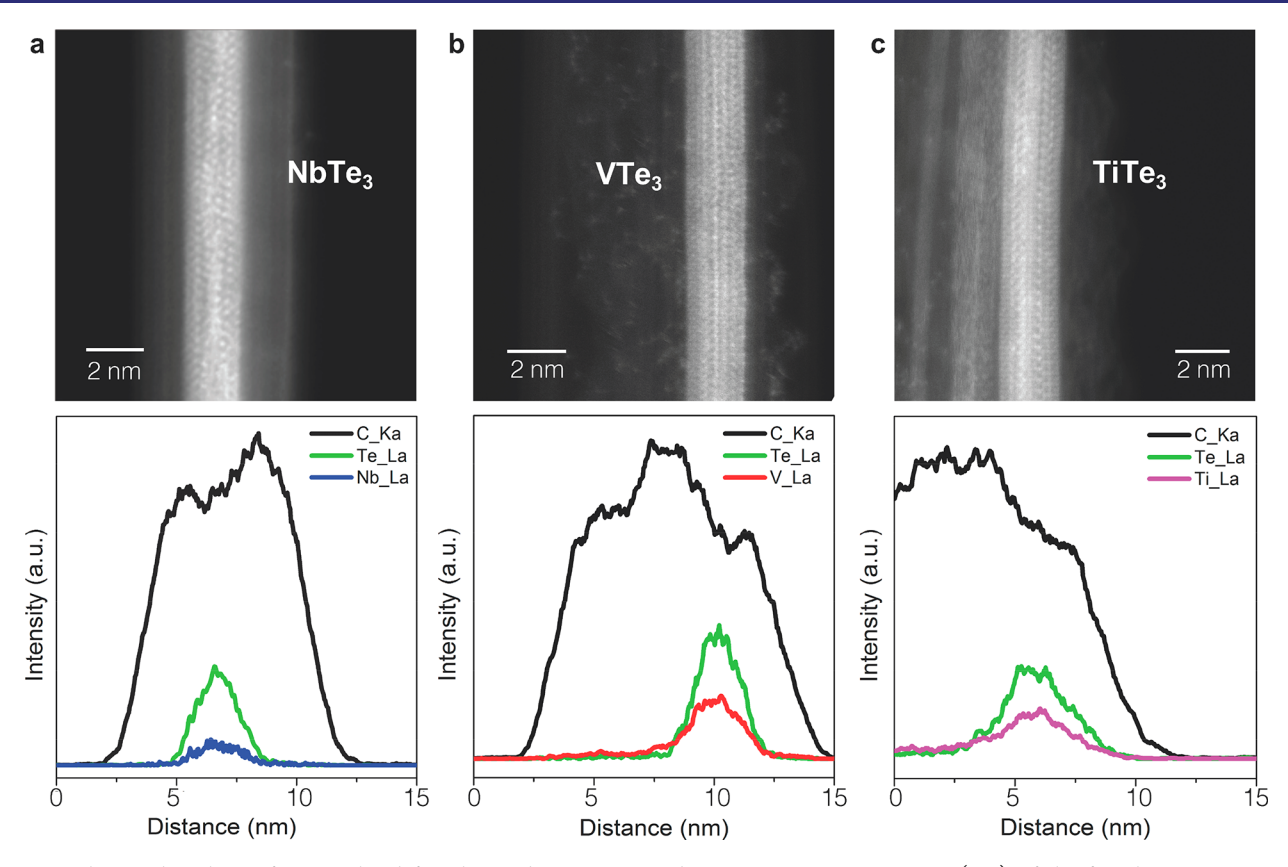


Figure 2. Elemental analysis of encapsulated few-chain NbTe<sub>3</sub>, VTe<sub>3</sub>, and TiTe<sub>3</sub>. ADF-STEM images (top) of the few-chain specimen, and corresponding EDS line scans for (a) NbTe<sub>3</sub>, (b) VTe<sub>3</sub>, and (c) TiTe<sub>3</sub>. EDS line scans (bottom) show the distribution of the transition metal and tellurium carbon within the carbon nanotube.

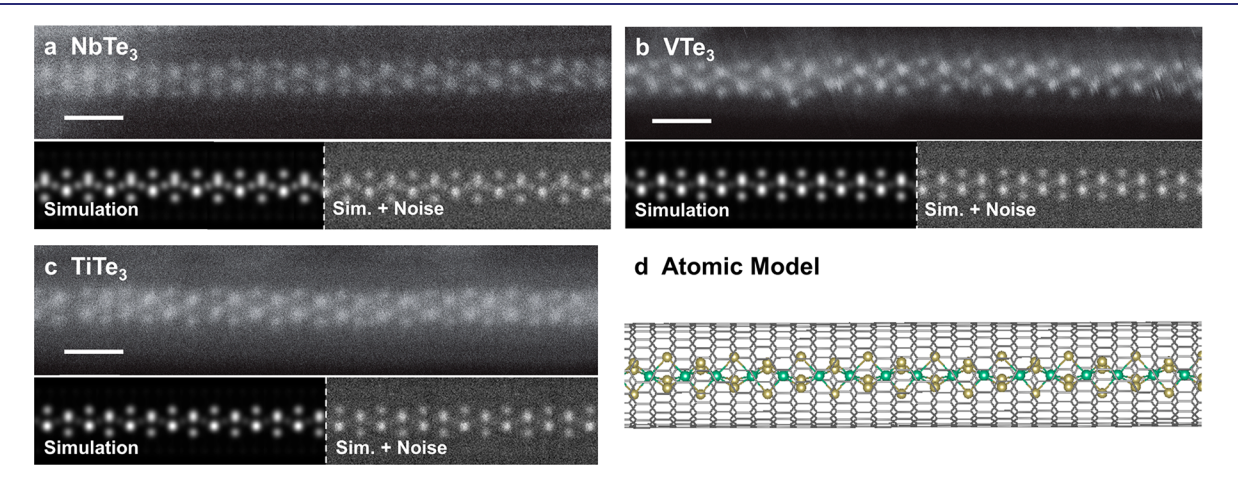


Figure 3. Single-chain STEM imaging, STEM simulation, and atomic structure of NbTe<sub>3</sub>, VTe<sub>3</sub>, and TiTe<sub>3</sub>. ADF-STEM images of single chains of encapsulated (a) NbTe<sub>3</sub>, (b) VTe<sub>3</sub>, and (c) TiTe<sub>3</sub>. Below each ADF-STEM image is the corresponding ADF-STEM image simulations (left) with appropriate noise from the microscope conditions added (right) from the structures obtained by DFT calculations (see Figure 4). Scale bars measure 1 nm. (d) Atomic structure and schematic of a single chain of transition metal tritelluride encapsulated within a carbon nanotube, where the gold and green atoms represent tellurium and the corresponding transition metal (Nb, V, or Ti), respectively, and the gray lattice represents the encapsulating CNT.

chain of encapsulated TiTe<sub>3</sub>, as titanium and hafnium are in the same group on the periodic table, so chemical trends imply this behavior. However, the TAP distortion seen in NbTe<sub>3</sub> and VTe<sub>3</sub> is surprising, as a previously studied encapsulated TMT in the same group, NbSe<sub>3</sub>, did not show the TAP distortion but rather a charge-induced torsional wave (CTW). Therefore, the TAP distortion seen in all three of these isolated structures could be closely related to their stability (or lack thereof) in

bulk crystals or indicate that this behavior is innate to the single-chain limit of transition metal tritellurides, which is studied in following sections.

We further investigate the structural makeup and the related TAP distortions of single-chain TiTe<sub>3</sub>, VTe<sub>3</sub>, and NbTe<sub>3</sub> via first-principles calculations based on density functional theory (DFT). As no bulk crystalline data are available for these TMT structures, we construct candidate structures for the chains

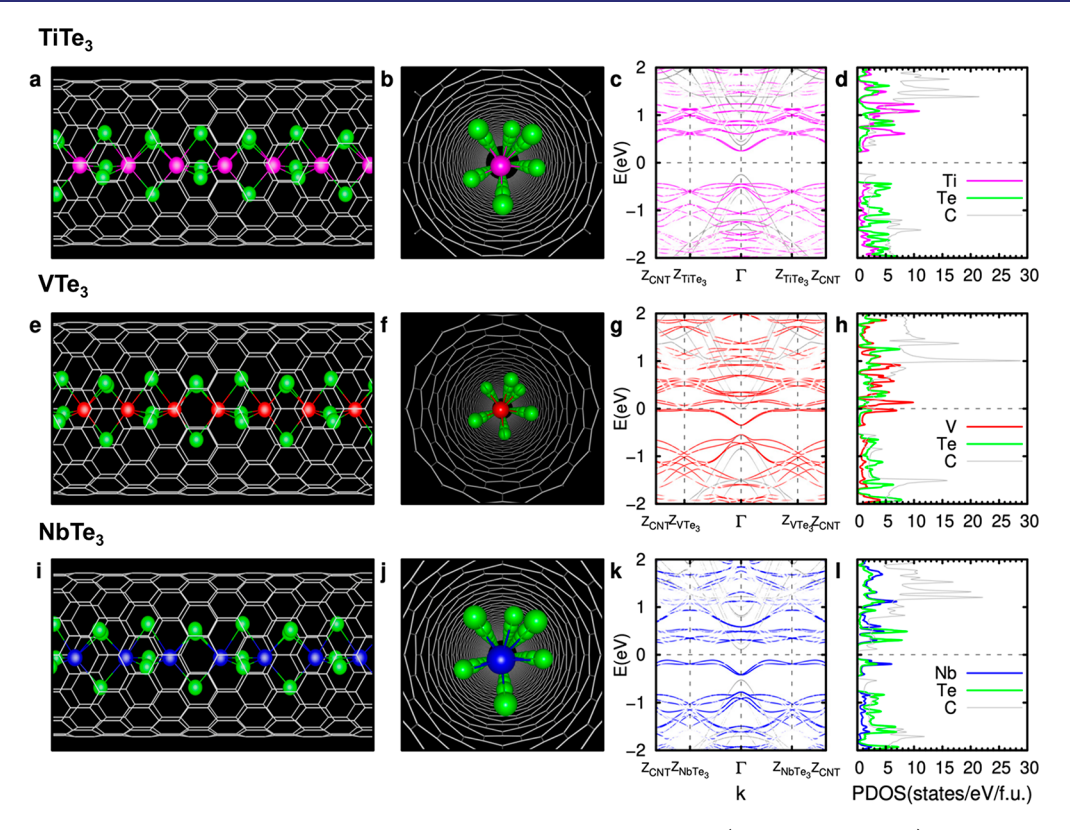


Figure 4. Calculated atomic structure and electronic structures for TAP single-chain MTe<sub>3</sub> (M = Ti, V, and Nb) encapsulated in CNT: (a–d) TiTe<sub>3</sub>, (e–h) VTe<sub>3</sub>, and (i–l) NbTe<sub>3</sub>. In the first and second columns, TAP single chains encapsulated inside a (14,0) CNT are presented side on and end on, respectively. In the atomic structure, the magenta, red, blue, and green spheres represent the Ti, V, Nb, and Te atoms, respectively. In the band structures, the chemical potential is set to zero and marked with a horizontal dashed line. In c, g, and k, the bands represented by magenta, red, blue, and gray lines are projected onto the single-chain TiTe<sub>3</sub>, VTe<sub>3</sub>, NbTe<sub>3</sub>, and CNT, respectively. Bands are then unfolded with respect to the first Brillouin zone of the unit cell of the single chain and the CNT, where zone boundaries for the chain and CNT are denoted as  $Z_{MTe_3}$  and  $Z_{CNT}$ , respectively. Here, the lengths of the first Brillouin zones of the TAP chains are one-half of those in the corresponding TP chains because of the doubled real-space unit cell length of the rocking chains, i.e.,  $Z_{MTe_3} = \pi/2 \cdot b_0^{MTe_3}$ , where  $b_0^{MTe_3}$  is the distance between the nearest transition metal atoms. In d, h, and l, the density of states projected onto Ti, V, Nb, Te, and C atoms are presented by magenta, red, blue, green, and gray lines, respectively.

with various symmetries including the TP and TAP phases (Figure S3). From the constructed candidate structures, the atomic structures are optimized by minimizing the total energy. In the optimization, the atomic positions are relaxed with the fixed value of the distance between the nearest transition metal atoms,  $b_0^{\rm MTe3}$  (M = Ti, V, and Nb), extracted from the STEM images shown in Figure 3.

We first consider the atomic and electronic structures of the single chains of TiTe<sub>3</sub>, VTe<sub>3</sub>, and NbTe<sub>3</sub> isolated in vacuum. The obtained atomic and electronic structures of the TP and TAP single chains isolated in vacuum are shown in Figures S4 and S5, respectively. All three of the TP single chains are metallic with Te bands crossing the Fermi level (Figure S4). For the TAP chains, the short-wavelength rocking distortions of Te ligands from a TP to a TAP unit cell, which was initially observed in the ADF-STEM images highlighted in Figure 3, lead to the split of the Te bands near the chemical potential (Figure S5). As a result, semiconducting band gaps of 0.690 and 0.486 eV in single chains of TiTe<sub>3</sub> (Figure S5c and S5d) and NbTe<sub>3</sub> (Figure S5k and S5l) are created, respectively, while the VTe<sub>3</sub> single chain remains metallic (Figure S5g and S5h). Note that the TAP structure of the single-chain TiTe<sub>3</sub> in vacuum has a 0.652 eV/formula unit (fu) lower energy than the TP structure in vacuum, while the TAP structures of the single chains of VTe<sub>3</sub> and NbTe<sub>3</sub> isolated in vacuum have

0.015 and 0.142 eV/fu higher energies than the TP structures in vacuum, respectively.

Next, we investigate the atomic and electronic structures of the single-chain TMT encapsulated inside a (14,0) CNT (indices chosen for convenience). We construct the candidate structures using the atomic positions of the single chains isolated in vacuum and those of the empty CNT. From the candidate structures the atomic positions of the chains are relaxed by minimizing the total energy, whereas the atomic positions of the CNT are fixed. The obtained atomic and electronic structures of the TP and TAP single chains of TMT species encapsulated in the CNT are shown in Figures S6 and 4, respectively. For the TP chains, all three of the MX<sub>3</sub> single chains remain metallic and the encapsulation does not alter the electronic structure of the chains significantly, except for the Fermi level shift due to the charge transfer between the chains and the CNT as shown in Figures S4 and S6. Figure 4 shows the obtained atomic structures, the electronic band structure, and the projected density of states (PDOS) for the TAP singlechain MX<sub>3</sub> encapsulated in the CNT. For the TAP single chains of the MX<sub>3</sub>, the encapsulation does not alter the electronic structure significantly, except for the chemical potential shift and the gap opening in the single-chain VTe<sub>3</sub> (Figures S5 and 4). The encapsulated TiTe<sub>3</sub> and NbTe<sub>3</sub> chains remain semiconducting with band gaps of 0.680 and 0.339 eV,

respectively, for the electron transfer within the chains. For VTe<sub>3</sub>, the encapsulation-driven band repulsion at the Fermi level around the zone boundary, Z<sub>VTe3</sub>, opens a band gap of 0.062 eV as shown in Figure 4 g and 4h, leading to a transition from metal to semiconductor. Note that the TAP structures of single-chain TiTe<sub>3</sub> and VTe<sub>3</sub> encapsulated in the CNT have 0.648 and 0.016 eV/formula unit (fu) lower energy than the TP structure encapsulated in the CNT, respectively, while the TAP structures of single-chain NbTe3 encapsulated in the CNT have 0.162 eV/fu higher energies than the TP structures encapsulated in the CNT. We calculate the binding energy,  $E_{\rm b}$ , of the single-chain MX<sub>3</sub>, which is defined as  $E_{\rm b} = E_{\rm MX3}^{\rm chain} + E_{\rm CNT} - E_{\rm MX3/CNT}$ , where  $E_{\rm MX3}^{\rm chain}$  is the total energy of the isolated single-chain MX<sub>3</sub>,  $E_{\rm CNT}$  is the total energy of an empty CNT isolated in vacuum, and  $E_{\rm MX3/CNT}$  is the total energy of the joint system of TP or TAP single-chain MX3 encapsulated inside the CNT. The calculated binding energies of the TAP (TP) single chains of TiTe<sub>3</sub>, VTe<sub>3</sub>, and NbTe<sub>3</sub> are 1.378 (1.381), 1.165 (1.134), and 1.384 (1.404) eV/fu, respectively.

Finally, we investigate the stability of the TMT families including these new materials by calculating the Gibbs free energies of formation,  $\delta G$ , of the MX<sub>3</sub>, which are defined as  $\delta G = \varepsilon_{\rm MX3} - n_{\rm M}\varepsilon_{\rm M} - n_{\rm X}\varepsilon_{\rm X}$ , where  $\varepsilon_{\rm MX3}$ ,  $\varepsilon_{\rm M}$ , and  $\varepsilon_{\rm X}$  are the total energies per atom of the bulk MX<sub>3</sub>, the bulk transition metal (M = Ti, Zr, Hf, V, Nb, and Ta), and the bulk chalcogen (X = S, Se, and Te), respectively, and  $n_{\rm M}$  and  $n_{\rm X}$  are the mole fractions of the M and X atoms, respectively. The calculated  $\delta G$ , as shown in Table 1, increases in the order of sulfide,

Table 1. Energetic Property of MX<sub>3</sub> Bulk,  $\delta G^a$ 

	Ti	Zr	Hf	V	Nb	Ta
S	-1.042	-1.110	-1.082	-0.650	-0.666	-0.690
Se	-0.829	-0.895	-0.870	-0.464	-0.560	-0.514
Te	-0.506	-0.653	-0.522	-0.156	-0.312	-0.163

<sup>a</sup>The Gibbs free energies of formation,  $\delta G$ , of the MX<sub>3</sub> is defined as  $\delta G = \varepsilon_{\text{MX3}} - n_{\text{M}}\varepsilon_{\text{M}} - n_{\text{X}}\varepsilon_{\text{X}}$ , where  $\varepsilon_{\text{MX3}}$ ,  $\varepsilon_{\text{M}}$ , and  $\varepsilon_{\text{X}}$  are the total energies per atom of the bulk MX<sub>3</sub>, the bulk transition metal M (M = Ti, Zr, Hf, V, Nb, and Ta), and the bulk chalcogen X (X = S, Se, and Te), respectively, and  $n_{\text{M}}$  and  $n_{\text{X}}$  are the mole fractions of the M and X atoms, respectively. The unit of δG is eV/atom.

selenide, and telluride compounds, possibly due to the size effect of the chalcogen atoms. The calculated  $\delta G$  of VTe<sub>3</sub> and NbTe<sub>3</sub> are -0.156 and -0.312 eV/atom, respectively, notably higher than those of the experimentally observed telluride materials, ZrTe<sub>3</sub> and HfTe<sub>3</sub>, which are -0.653 and -0.522 eV/ atom, respectively, while that of TiTe3 is -0.506 eV/atom, comparable with those of ZrTe3 and HfTe3. We compare the stability of an MX<sub>3</sub> configuration with those of an MX<sub>2</sub> configuration by calculating  $\Delta E$ , which is defined as  $\Delta E = E_{\text{MX3}}^{\text{bulk}} - E_{\text{MX2}}^{\text{bulk}} - E_{\text{X}}^{\text{bulk}}$ , where  $E_{\text{MX3}}^{\text{bulk}}$ ,  $E_{\text{MX2}}^{\text{bulk}}$ , and  $E_{\text{X}}^{\text{bulk}}$  are the total energies of the bulk MX<sub>3</sub>, MX<sub>2</sub>, and X, respectively. The calculated  $\Delta E$  of TiTe<sub>3</sub>, VTe<sub>3</sub>, and NbTe<sub>3</sub> are 0.193, 0.292, and 0.110 eV/fu, respectively, meaning the MX<sub>3</sub> configurations are less stable than the MX<sub>2</sub> configurations, while those of TaS₃, NbSe₃, and ZrTe₃ are −0.155, -0.063, and -0.011 eV/fu, respectively, meaning the MX<sub>3</sub> configurations have higher or comparable stability compared to the MX<sub>2</sub> configurations. On the basis of the calculated  $\delta G$  and  $\Delta E$ , VTe<sub>3</sub> has the lowest  $\delta G$  and highest  $\Delta E$ , implying it is the hardest to achieve in bulk form. However, NbTe<sub>3</sub> and TiTe<sub>3</sub> are also difficult to realize in their bulk form due to low  $\delta G$  and

 $\delta E$ , respectively. This is consistent with there being no reports of successful bulk synthesis of these materials.

#### CONCLUSION

In summary, we have demonstrated the few- and single-chain limit synthesis of three new members of the quasi-1D TMT family via encapsulation within the hollow cavity of MWCNTs. The nanotube sheath stabilizes and protects the materials, allowing access to hitherto unseen compositions and crystal structures, specifically NbTe<sub>3</sub>, VTe<sub>3</sub>, and TiTe<sub>3</sub>. We investigated the structures of the new materials with atomicresolution electron microscopy, revealing interesting structural anomalies, including a trigonal antiprismatic rocking distortion in single-chain specimen. DFT calculations illuminate the electronic properties of single chains of the materials encapsulated in MWCNTs and quantify the stability of these materials in their bulk form and in the single-chain limit. Our study lays further groundwork for the study of confinementstabilized nonequilibrium materials and associated emergent physical phenomena.

#### ASSOCIATED CONTENT

# **Solution** Supporting Information

The Supporting Information is available free of charge at https://pubs.acs.org/doi/10.1021/jacs.0c10175.

Electron microscopy details for experimental STEM imaging and STEM simulations, and details on computational methods used (PDF)

### AUTHOR INFORMATION

# **Corresponding Author**

Alex Zettl — Department of Physics, University of California at Berkeley, Berkeley, California 94720, United States; Kavli Energy NanoSciences Institute at the University of California at Berkeley, Berkeley, California 94720, United States; Materials Sciences Division, Lawrence Berkeley National Laboratory, Berkeley, California 94720, United States; orcid.org/0000-0001-6330-136X; Email: azettl@berkeley.edu

## **Authors**

Scott Stonemeyer — Department of Physics and Department of Chemistry, University of California at Berkeley, Berkeley, California 94720, United States; Kavli Energy NanoSciences Institute at the University of California at Berkeley, Berkeley, California 94720, United States; Materials Sciences Division, Lawrence Berkeley National Laboratory, Berkeley, California 94720, United States; orcid.org/0000-0002-8135-5625

Jeffrey D. Cain — Department of Physics, University of California at Berkeley, Berkeley, California 94720, United States; Kavli Energy NanoSciences Institute at the University of California at Berkeley, Berkeley, California 94720, United States; Materials Sciences Division, Lawrence Berkeley National Laboratory, Berkeley, California 94720, United States; Occid.org/0000-0001-9244-4271

Sehoon Oh — Department of Physics, University of California at Berkeley, Berkeley, California 94720, United States; Materials Sciences Division, Lawrence Berkeley National Laboratory, Berkeley, California 94720, United States; orcid.org/0000-0003-0518-4091

Amin Azizi – Department of Physics, University of California at Berkeley, Berkeley, California 94720, United States; Kavli

- Energy NanoSciences Institute at the University of California at Berkeley, Berkeley, California 94720, United States
- Malik Elasha Department of Physics, University of California at Berkeley, Berkeley, California 94720, United States
- Markus Thiel Department of Physics, University of California at Berkeley, Berkeley, California 94720, United States
- Chengyu Song Materials Sciences Division, Lawrence Berkeley National Laboratory, Berkeley, California 94720, United States; National Center for Electron Microscopy, The Molecular Foundry, Berkeley, California 94720, United States
- Peter Ercius Materials Sciences Division, Lawrence Berkeley National Laboratory, Berkeley, California 94720, United States; National Center for Electron Microscopy, The Molecular Foundry, Berkeley, California 94720, United States; © orcid.org/0000-0002-6762-9976
- Marvin L. Cohen Department of Physics, University of California at Berkeley, Berkeley, California 94720, United States; Materials Sciences Division, Lawrence Berkeley National Laboratory, Berkeley, California 94720, United States

Complete contact information is available at: https://pubs.acs.org/10.1021/jacs.0c10175

#### **Author Contributions**

\*S.S., J.C., and S.O. contributed equally.

#### **Funding**

This work was primarily funded by the U.S. Department of Energy, Office of Science, Office of Basic Energy Sciences, Materials Sciences and Engineering Division under Contract No. DE-AC02-05-CH11231 within the sp2-Bonded Materials Program (KC2207) which provided for synthesis of the compounds, TEM and STEM structural characterization, and theoretical modeling. The elemental mapping work was funded by the U.S. Department of Energy, Office of Science, Office of Basic Energy Sciences, Materials Sciences and Engineering Division under Contract No. DE-AC02-05-CH11231 within the van der Waals Heterostructures Program (KCWF16). Work at the Molecular Foundry (TEAM 0.5 characterization) was supported by the Office of Science, Office of Basic Energy Sciences, U.S. Department of Energy under Contract No. DE-AC02-05-CH11231. Support was also provided by the National Science Foundation under Grant Nos. DMR-1807233, which provided for preparation of opened nanotubes, and DMR-1926004, which provided for theoretical calculations of the electronic and structural properties. Computational resources were provided by the DOE at Lawrence Berkeley National Laboratory's NERSC facility and the NSF through XSEDE resources at NICS.

#### Notes

The authors declare no competing financial interest.

# **■** REFERENCES

- (1) Novoselov, K. S.; Geim, A. K.; Morozov, S. V.; Jiang, D.; Zhang, Y.; Dubonos, S. V.; Grigorieva, I. V.; Firsov, A. A. Electric Field in Atomically Thin Carbon Films. *Science (Washington, DC, U. S.)* **2004**, 306 (5696), 666–669.
- (2) Splendiani, A.; Sun, L.; Zhang, Y.; Li, T.; Kim, J.; Chim, C. Y.; Galli, G.; Wang, F. Emerging Photoluminescence in Monolayer MoS 2. *Nano Lett.* **2010**, *10* (4), 1271–1275.

- (3) Pham, T.; Oh, S.; Stetz, P.; Onishi, S.; Kisielowski, C.; Cohen, M. L.; Zettl, A. Torsional Instability in the Single-Chain Limit of a Transition Metal Trichalcogenide. *Science (Washington, DC, U. S.)* **2018**, *361* (6399), 263–266.
- (4) Pham, T.; Oh, S.; Stonemeyer, S.; Shevitski, B.; Cain, J. D.; Song, C.; Ercius, P.; Cohen, M. L.; Zettl, A. Emergence of Topologically Nontrivial Spin-Polarized States in a Segmented Linear Chain. *Phys. Rev. Lett.* **2020**, 124 (20), 206403.
- (5) Al Balushi, Z. Y.; Wang, K.; Ghosh, R. K.; Vilá, R. A.; Eichfeld, S. M.; Caldwell, J. D.; Qin, X.; Lin, Y.-C.; Desario, P. A.; Stone, G.; Subramanian, S.; Paul, D. F.; Wallace, R. M.; Datta, S.; Redwing, J. M.; Robinson, J. A. Two-Dimensional Gallium Nitride Realized via Graphene Encapsulation. *Nat. Mater.* **2016**, *15* (11), 1166–1171.
- (6) Briggs, N.; Bersch, B.; Wang, Y.; Jiang, J.; Koch, R. J.; Nayir, N.; Wang, K.; Kolmer, M.; Ko, W.; De La Fuente Duran, A.; Subramanian, S.; Dong, C.; Shallenberger, J.; Fu, M.; Zou, Q.; Chuang, Y.-W.; Gai, Z.; Li, A.-P.; Bostwick, A.; Jozwiak, C.; Chang, C.-Z.; Rotenberg, E.; Zhu, J.; van Duin, A. C. T.; Crespi, V.; Robinson, J. A. Atomically Thin Half-van Der Waals Metals Enabled by Confinement Heteroepitaxy. *Nat. Mater.* 2020, 19 (6), 637–643.
- (7) Pham, T.; Fathalizadeh, A.; Shevitski, B.; Turner, S.; Aloni, S.; Zettl, A. A Universal Wet-Chemistry Route to Metal Filling of Boron Nitride Nanotubes. *Nano Lett.* **2016**, *16* (1), 320–325.
- (8) Flahaut, E.; Sloan, J.; Friedrichs, S.; Kirkland, A. I.; Coleman, K. S.; Williams, V. C.; Hanson, N.; Hutchison, J. L.; Green, M. L. H. Crystallization of 2H and 4H PbI2 in Carbon Nanotubes of Varying Diameters and Morphologies. *Chem. Mater.* **2006**, *18* (8), 2059–2069.
- (9) Sloan, J.; Grosvenor, S. J.; Friedrichs, S.; Kirkland, A. I.; Hutchison, J. L.; Green, M. L. H. A One-Dimensional Bal2 Chain with Five- and Six-Coordination, Formed within a Single-Walled Carbon Nanotube. *Angew. Chem., Int. Ed.* **2002**, *41* (7), 1156–1159.
- (10) Nagata, M.; Shukla, S.; Nakanishi, Y.; Liu, Z.; Lin, Y.-C.; Shiga, T.; Nakamura, Y.; Koyama, T.; Kishida, H.; Inoue, T.; Kanda, N.; Ohno, S.; Sakagawa, Y.; Suenaga, K.; Shinohara, H. Isolation of Single-Wired Transition-Metal Monochalcogenides by Carbon Nanotubes. *Nano Lett.* **2019**, *19* (8), 4845–4851.
- (11) Carter, R.; Sloan, J.; Kirkland, A. I.; Meyer, R. R.; Lindan, P. J. D.; Lin, G.; Green, M. L. H.; Vlandas, A.; Hutchison, J. L.; Harding, J. Correlation of Structural and Electronic Properties in a New Low-Dimensional Form of Mercury Telluride. *Phys. Rev. Lett.* **2006**, *96* (21), 215501.
- (12) Spencer, J. H.; Nesbitt, J. M.; Trewhitt, H.; Kashtiban, R. J.; Bell, G.; Ivanov, V. G.; Faulques, E.; Sloan, J.; Smith, D. C. Raman Spectroscopy of Optical Transitions and Vibrational Energies of ~ 1 Nm Hgte Extreme Nanowires within Single Walled Carbon Nanotubes. *ACS Nano* **2014**, *8* (9), 9044–9052.
- (13) Philp, E.; Sloan, J.; Kirkland, A. I.; Meyer, R. R.; Friedrichs, S.; Hutchison, J. L.; Green, M. L. H. An Encapsulated Helical One-Dimensional Cobalt Iodide Nanostructure. *Nat. Mater.* **2003**, *2* (12), 788–791.
- (14) Grüner, G.; Zettl, A.; Clark, W. G.; Thompson, A. H. Observation of Narrow-Band Charge-Density-Wave Noise in TaS3. *Phys. Rev. B: Condens. Matter Mater. Phys.* **1981**, 23, 6813–6815.
- (15) Li, J.; Peng, J.; Zhang, S.; Chen, G. Anisotropic Multichain Nature and Filamentary Superconductivity in the Charge Density Wave System HfTe3. *Phys. Rev. B: Condens. Matter Mater. Phys.* **2017**, 96 (17), 1–8.
- (16) Meyer, S.; Pham, T.; Oh, S.; Ercius, P.; Kisielowski, C.; Cohen, M. L.; Zettl, A. Metal-Insulator Transition in Quasi-One-Dimensional HfTe3 in the Few-Chain Limit. *Phys. Rev. B: Condens. Matter Mater. Phys.* **2019**, *100* (4), 041403.
- (17) Canadell, E.; Jobic, S.; Brec, R.; Rouxel, J. Electronic Structure and Properties of Anionic Mixed Valence and Layered CrTe3: The Question of Extended Tellurium Bonding in Transition Metal Tellurides. *J. Solid State Chem.* **1992**, *98* (1), 59–70.
- (18) Kirkland, E. J. Advanced Computing in Electron Microscopy; Springer International Publishing, 2020. DOI: 10.1007/978-3-030-33260-0.